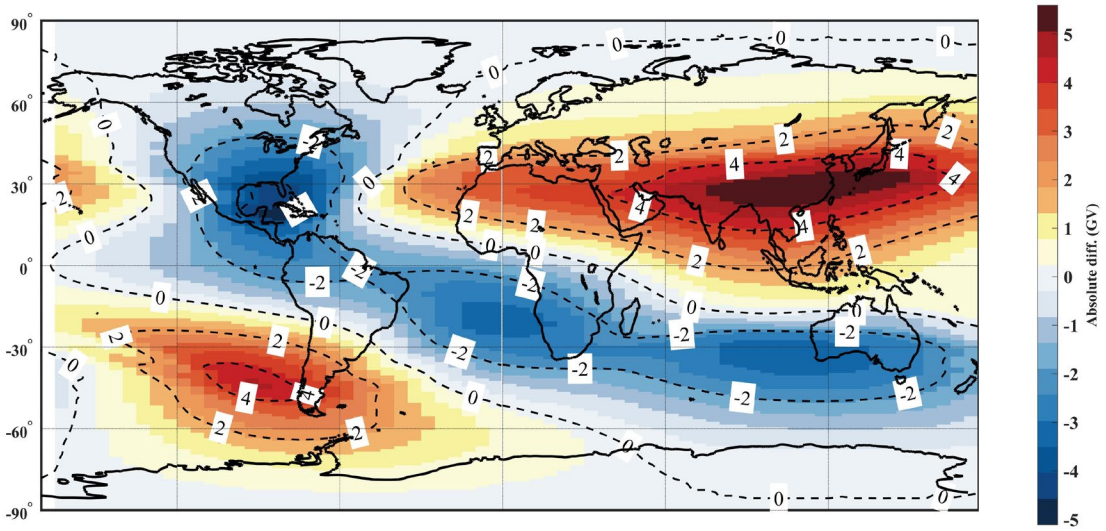

Figure S1. Differences between cut-off rigidity from Copeland (2018) and cut-off rigidity using the Stoermer approximation.

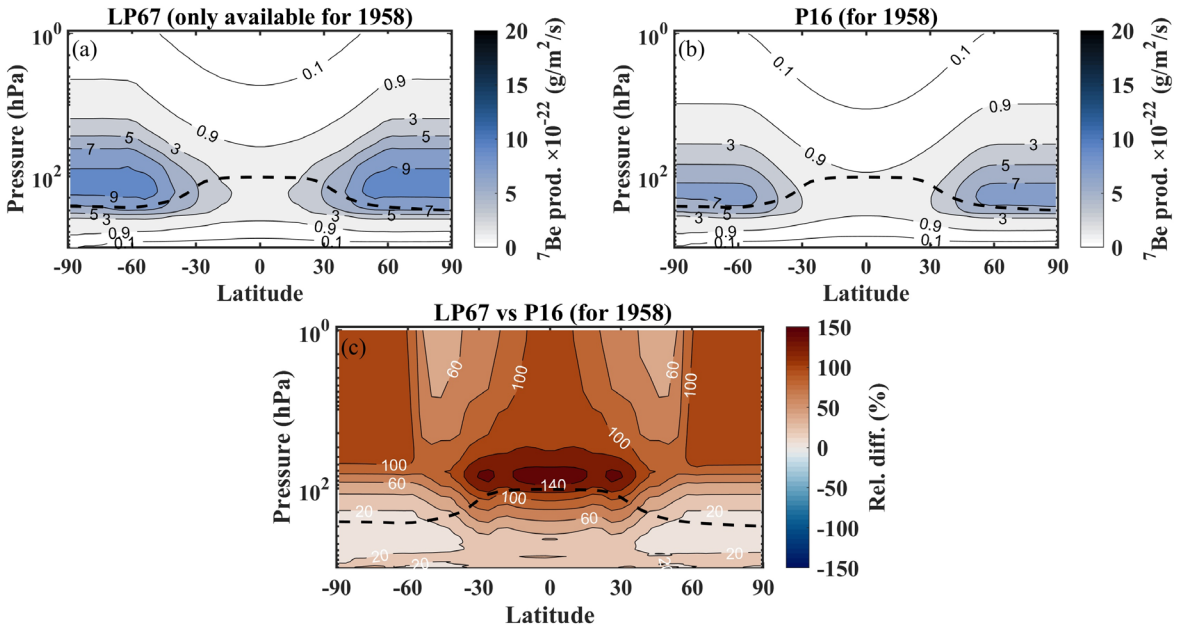

Figure S2. ^{7}Be production rates of (a) LP67 for the year 1958, (b) P16 for the year 1958, and (c) relative differences (%) between LP67 and P16 production rates for the year 1958, i.e., (^{7}Be$_{LP67}$-^{7}Be$_{P16}$)/ ^{7}Be$_{P16}$×100%. The dashed line indicates the location of MERRA-2 thermal tropopause.

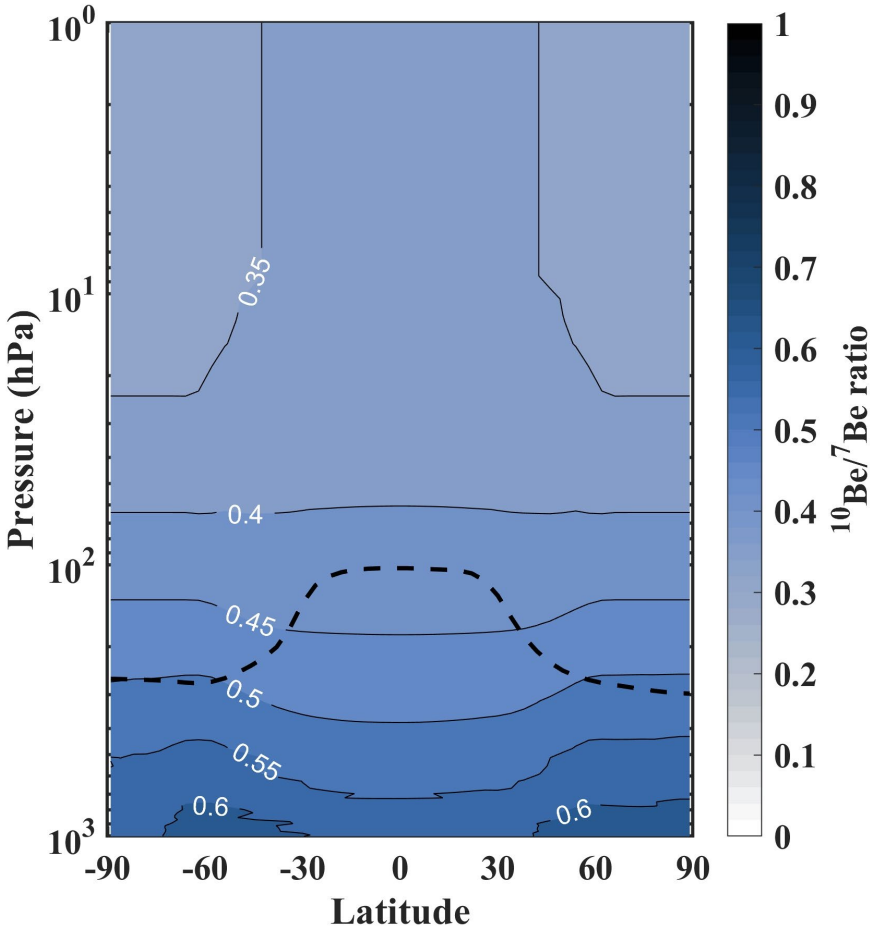

Figure S3. Vertical distribution of the ^{10}Be/^{7}Be production ratios derived from the P16 production model. The black dash line indicates the location of MERRA-2 thermal tropopause.

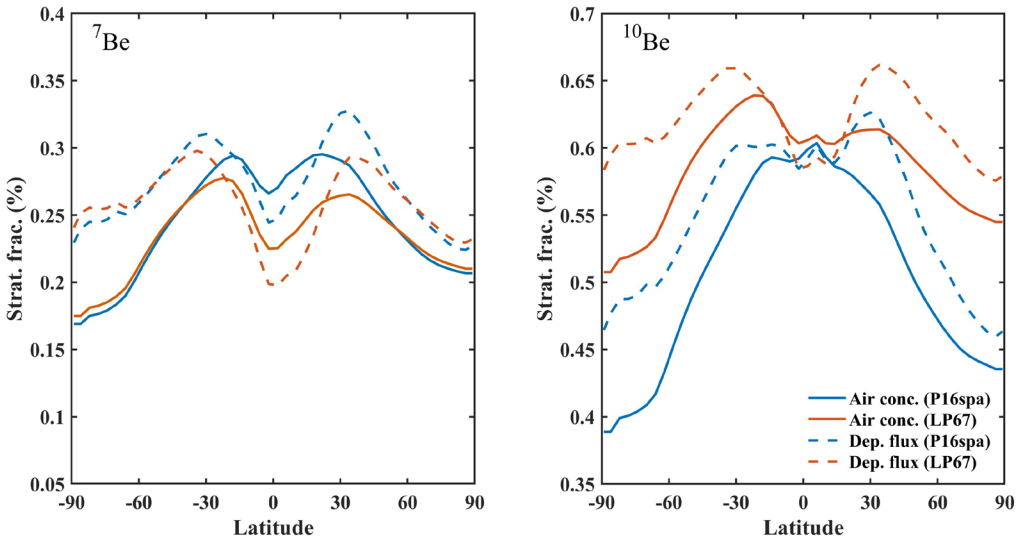

Figure S4. Stratospheric fraction of annual zonal mean surface air concentrations (solid lines) and total deposition fluxes (dashed lines) in the model simulations as a function of latitude for ^{7}Be (left panel) and ^{10}Be (right panel).

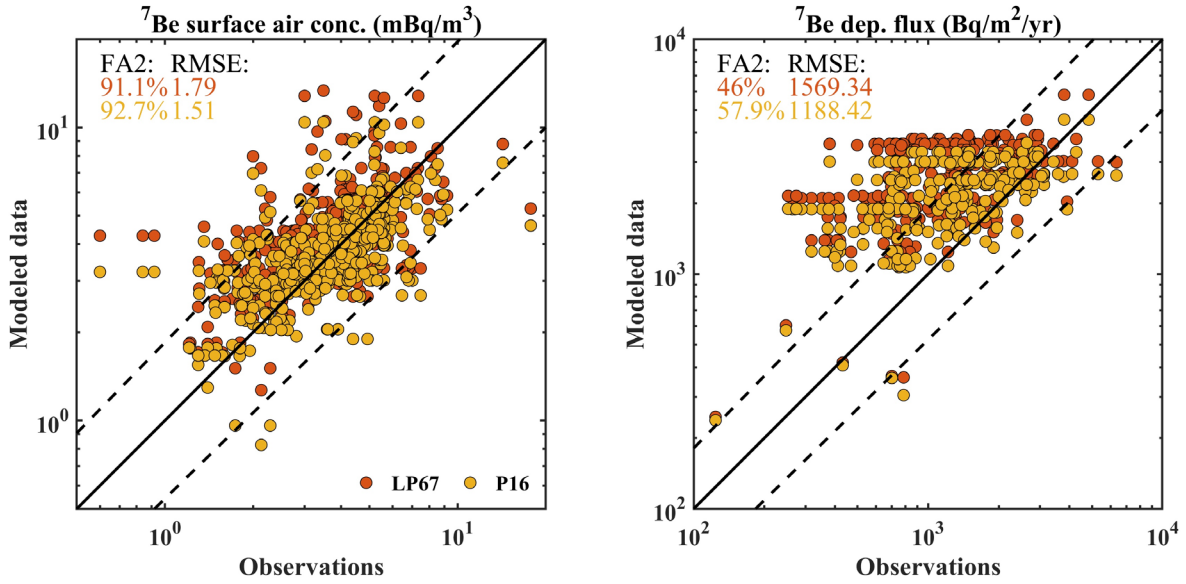

Figure S5. Scatter plot of modeled $^7Be_{LP67}$ (red color) and $^7Be_{P16}$ (orange color) versus observed ^{7}Be surface air concentrations (left panel) and deposition fluxes (right panel). The dashed lines are the factor of 2 of 1:1 line (straight lines). Noted that $^7Be_{LP67}$ is multiplied with a scale factor (1.39) to correct the solar modulation influence following previous studies (e.g., Koch et al., 1996; Liu et al., 2016)

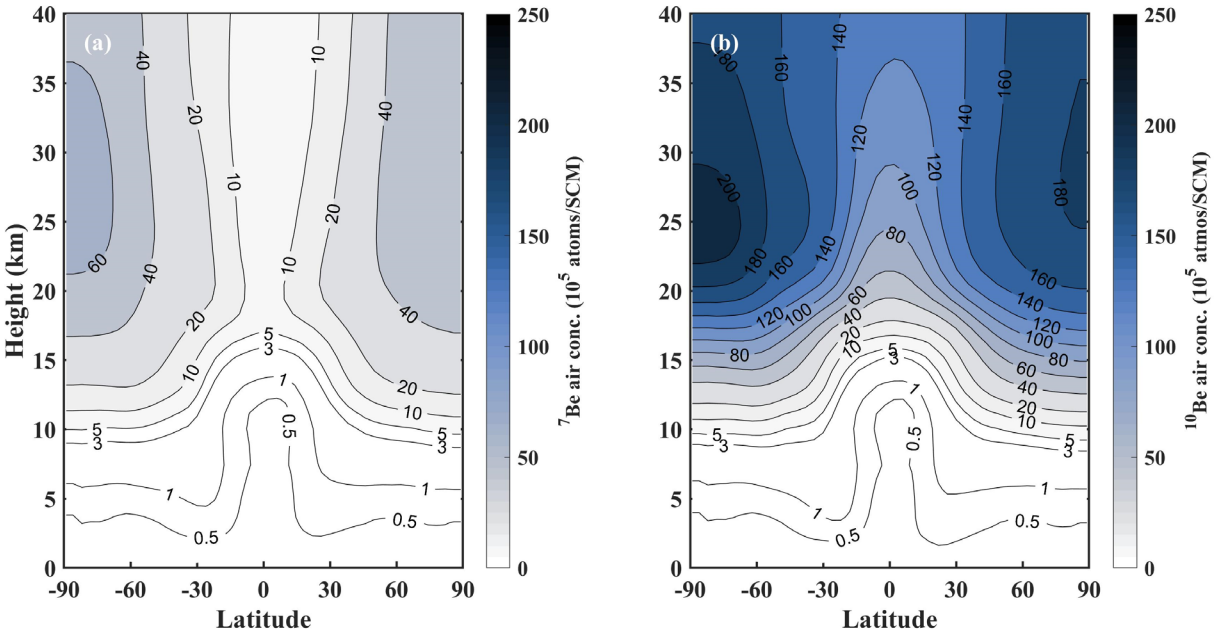

Figure S6. Latitude-height cross-sections of model zonal mean (a) ^{7}Be$_{P16spa}$ and (b) ^{10}Be$_{P16spa}$ ($\times 10^5$ atoms/SCM) over the period 2008-2018.

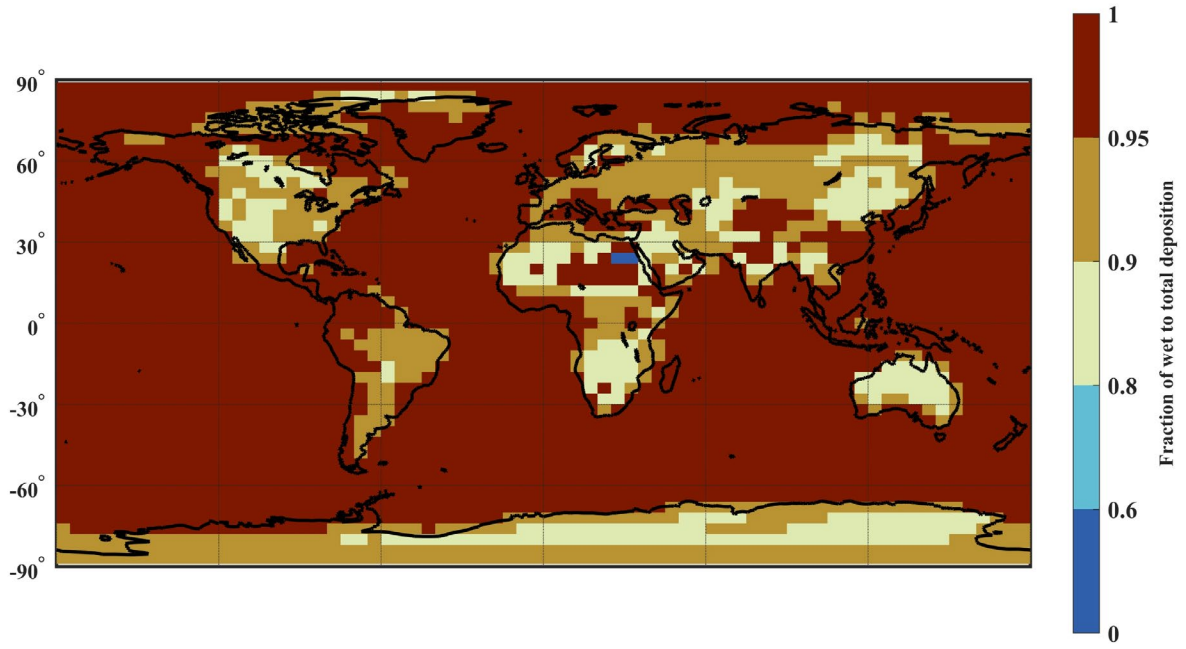

Figure S7. Fractions of wet to total deposition fluxes of $^{10}Be_{P16spa}$ modeled by GEOS-Chem averaged over the period 2008-2018. Noted that this fraction is also similar for modeled $^{7}Be_{P16spa}$.